PREDICTION OF SATELLITE CLOUD PATTERNS

USING SPATIAL FOURIER TRANSFORMS

by

Howard Bruce Bluestein

S.B., Massachusetts Institute of Technology, (1971)

SUBMITTED IN PARTIAL FULFILLMENT OF THE
REQUIREMENTS FOR THE DEGREE OF
MASTER OF SCIENCE

at the

MASSACHUSETTS INSTITUTE OF TECHNOLOGY

Signature of Author . . . . . .
Department of Meteorology

Certified by . . . . . .
Thesis Supervisor

Accepted by . . . . . .
Chairman, Departmental Committee on
Graduate Students

PREDICTION OF SATELLITE CLOUD PATTERNS USING SPATIAL FOURIER TRANSFORMS

by

Howard B. Bluestein

Submitted jointly to the Department of Meteorology and the Department of Electrical Engineering on 14 April 1972 in partial fulfillment of the requirements for the degree of Master of Science.

ABSTRACT

A method for forecasting filtered satellite cloud patterns using spatial Fourier transforms is devised. Two prediction formulae are formulated: one is in effect a forecast of "persistence" of phase speed of the Fourier components in addition to an exponential extrapolation of their intensity; the other is only a forecast of "persistence" of phase speed of the Fourier components. Error analysis includes root-mean-square computations in addition to a comparison of predicted, climatological and actual cloud motions. For the single forecast, the prediction of only "persistence" of phase speed was the better forecast, but it still failed to do as well as simple persistence of the pattern.

Thesis Supervisors: Frederick Sanders, Professor of Meteorology
Edward N. Lorenz, Professor of Meteorology
Oleh Tretiak, Research Associate, Electrical Engineering

Table of Contents

Introduction

Prediction of satellite cloud patterns has until now involved only the motion of either an entire cloud mass or of certain individual features of a cloud mass. A cloud mass may be defined as a readily distinguishable shape of cloud. For example, a circular disk with bands, such as a tropical cyclone, a long band such as that associated with a mid-latitude front, an "inverted-V" banded structure such as a tropical wave, a "speckled" area indicative of small scale convection, and a band such as the Intertropical Convergence Zone, are all quite distinct cloud masses.

The simplest form of prediction is extrapolation of cloud motion by estimating cloud speed (Hubert and Whitney, 1971). This is done by preparing a movie sequence by photographing individual images that were taken at fixed time intervals by a geosynchronous satellite. The movie sequence is projected repeatedly onto a worksheet by means of an endless loop. The initial and final positions of selected regions of the cloud, plus scaling information, and the known time interval between pictures enable one to determine cloud velocity vectors.

One objective way of determining cloud motion is via a cross-correlation technique (Leese, Novak and Taylor; Leese, Novak, Clark, 1971). A satellite picture is a two dimensional array of points, each point of which represents a sample of the intensity (reflectance) of cloud material at that point on Earth. One defines the covariance cov(p,q) between two pictures covering the same region on Earth, where p and q are the displacements for x and y. The images are taken at different times t_0 and t_1, however. Δx and Δy are the sampling intervals, and Δt is the time interval between

the two pictures. Having found the displacements p' and q' which maximize cov (p,q), one may determine the speed C and direction of motion θ via the following relation:

$$c = \frac{\left[(p'\Delta x)^2 + (q'\Delta y)^2\right]^{1/2}}{\Delta t}$$

$$\theta = \tan^{-1} \frac{p'\Delta x}{q'\Delta y}$$

The actual computation of the covariance function is done in the frequency domain by obtaining the two-dimensional discrete Fourier transform of both images, multiplying one transform by the complex-conjugate of the other transform, and inverse-transforming.

Another objective method of determining cloud motion is through "binary matching" (Leese, Novak and Taylor, 1970). Whereas the correlation technique required all the image's gray-scale information, the binary matching scheme assigns a level one or level zero according to the existence or nonexistence of a feature such as an edge, a closed region, etc. For example, the cloud area may be represented by a level one and the complement of the cloud may be represented by a level zero. When a sequence of two images are superposed, areas of overlap can be represented by one shading, while cloud free areas can be represented by another shading. The displacement of the clouds can be deduced by measuring the distance between the leading edge of a cloud area and the overlapping regions. One may also locate centers of brightness, chosen on the basis of area and brightness (analogous to centers of mass in mechanics)(Endlich, Wolf, Hall and Brain, 1971). Again, the motion field may be inferred by measuring the

displacement of centers in successive photographs. Results indicate that the computer techniques were at least as good as manual techniques such as use of film loops .

The preceding methods of computing wind fields have two major weaknesses: one does not know the height of the tops of the clouds, and therefore the measured displacement field may be valid either for some unknown level in the atmosphere or for different unknown levels in the atmosphere; the second source of difficulty lies in non-advective cloud motion, i.e. in clouds which do not move along with the flow at their height. On time scales of less than thirty minutes, certain cumulus clouds may disappear, and subsequently others may reappear at some distance from the initial cumulus cloud band, thus leading one to an overestimation of cloud motion.

The analogous problem of prediction of radar precipitation echoes has been investigated via linear regression (Noel and Fleisher, 1960). The following prediction equation was used:

$$I_m(t + n\Delta t) = A_o^m + \sum_1^N A_k^m I_k(t) + \mathcal{E}_m(t)$$

where $I_m(t+n\Delta t)$ in the signal intensity (radar reflectance at station m, at time $t+n\Delta t$; I_k (t) are all the observations at all k stations.

$n\Delta t$ is the forecast time and Δt = 10 minutes

A_o^m , A_k^m are constants to be determined.

E_m (t) is the error from predictions.

The constants A_o^m and A_k^m were found by minimizing $\overline{\mathcal{E}_m^2(t)}$ with respect to A_k^m. The difference between $\overline{I_m^2(t+n\Delta t)}$, the variance of the predictand, and $\overline{\mathcal{E}_m^2(t)}$, the variance of the error, divided by $\overline{I_m^2(t+n\Delta t)}$, the variance of the error is an objective measure of the effectiveness of the prediction. This ratio is the reduction in variance, where high reductions in variance indicate good predictions and vice versa. The prediction equation was good only for forecasts of less than ten minutes. Ten minutes is perhaps one-third to one-half the total lifetime of a radar cell of identifiable character. One would hope then that a satellite cloud prediction also is possible for one-third to one-half the total lifetime of an identifiable cloud mass.

One could hope to infer something more from sequences of satellite cloud patterns than just simple cloud motions. Assuming that the physical laws which dictate what type of cloud pattern changes will occur from one time to another do not change with time, one could try to deduce an empirical formula for prediction of future cloud changes. This prediction would be made without a direct knowledge of the dynamical processes which sustain the cloud pattern.

On the other hand, one <u>can</u> deduce some dynamical processes from sequences of pictures. An area of cumulus convection appearing as bands or cells may, via physical processes which are not well understood, "blow up" into larger scale systems, as evidenced by an extensive cirrus canopy and cirrus blowoff. The sharpness of cloud mass boundaries may give clues as to the modes of vertical motion near the disturbance. For example, sharp cloud edges may suggest strong subsidence around the clouds. Overall

cloud shape may give some hint as to the presence of large-scale waves. The diameter of bright storm shields composed of integrated thunderstorm anvils may be used as an index of storm severity (Boucher, 1967). One is therefore justified in believing that the near-past history of cloud pattern may be of some use in predicting future patterns.

The purpose of this thesis, then, is to formulate a prediction formula which describes the motion and shape change of cloud masses. This differs from previous works in which trackable entities of cloud patterns were used to infer the wind field at some level in the atmosphere. Instead of looking at individual cloud elements, one considers the gross aspects of the cloud mass such as shape, texture, and sharpness of cloud boundaries. The results of the prediction formula will be evaluated by comparing the motions of the more gross features of the image with the predicted motions and with the climatological motions, and by considering the root-mean-square error of the prediction.

It is shown later that one justification for seeking prediction formulae of cloud motion is that conventional meteorological data are quite sparse in certain regions of the globe such as the topics. Satellite observations, however, are currently quite plentiful for the tropics, a region which is less well-understood than others.

Studies of tropical disturbances (Reed and Recker, 1971) until now, for example, concentrated on case studies using synoptic methods, e.g. (Riehl, 1945), spectral and cross-spectral analysis of meteorological variables, e.g. (Yanai, 1968), averages of satellite pictures, e.g. (Wallace, 1970), and theoretical studies based on the dynamic equations, e.g. (Yanai and Nitta, 1967).

One major difficulty in tracking these disturbances through the tropics is that while they might possess nearly the same amplitude and wind field from day to day, the modes (i.e. scales and shapes) of convective areas do definitely change. What dynamic processes cause these changes are not exactly known, but perhaps an attempt to predict changes might be useful. For example, a successful prediction without any knowledge of the physics involved might imply that there is something very important about the mode of convection which dictates what sustains or weakens the disturbance.

I therefore felt well justified in attempting my prediction formula on a feature in the tropics such as a tropical wave, as a new method of analysis.

Formulation of the Prediction Equation

Rather than consider the satellite cloud patterns in the spatial domain, one can consider the patterns in the frequency domain (two-dimensional Fourier transform of the cloud pattern). Results of past experiments (Leese and Epstein, 1963) characterized by low resolution of size and brightness scales, suggest that some features can be revealed in the frequency domain which were obscured by the more dominant features in the spatial domain. The problem therefore may be stated as the following: one is given satellite cloud photographs of the reflectance field a (x,y) (A photograph of the reflectance field is hereafter referred to as a photograph) at time $t = -\Delta t$, b (x,y) at time $t = 0$, and the "verification" c_v (x,y) (verification arrays will be denoted by a subscript v; predictand arrays will be denoted by a subscript p), i.e. the cloud pattern at $t = +\Delta t$. The process of change from a (x,y) to b (x,y) may be characterized by an operator 0, such

that $O[a(x,y)] = b(x,y)$. Assuming that O does not change with time, one can expect that, likewise,

$$O[b(x,y)] = c_v(x,y).$$

O must be found. The function or functional that represents O might be found in a way unlike that associated with linear regression or binary matching.

Consider the problem of determining an inverse filter in restoring atmospherically degraded photographs (Huang, Schreiber, Tretiak, 1971); one has the blurred image b(x,y) and the impulse response of the atmosphere, h(x,y), i.e. the blurred photograph of a star which acts like a point source or an impulse in space. Given that $O[a(x,y)] = b(x,y)$ where a(x,y) is the original unblurred image, then one can assume that O is the convolution of h(x,y) with the "input" unblurred image. This relation implies linearity and shift invariance of the system, i.e. for "inputs" a_1 and a_2 corresponding to outputs b_1 and b_2, and for constants β_1 and β_2 γ_1 and γ_2, γ_3 and γ_4:

$$O\left[\beta_1 a_1(x-\gamma_1, y-\gamma_2) + \beta_2 a_2(x-\gamma_3, y-\gamma_4)\right] =$$

$$\beta_1 b_1(x-\gamma_1, y-\gamma_2) + \beta_2 b_2(x-\gamma_3, y-\gamma_4)$$

So,

$$b(x,y) = \int_{-\infty}^{\infty}\int_{-\infty}^{\infty} a(\alpha-x, \beta-y)\, h(\alpha,\beta)\, d\alpha\, d\beta$$

In the frequency domain,

$B(f_x,f_y) = A(f_x,f_y)H(f_x,f_y)$ where f_x, f_y are the horizontal and vertical

spatial frequencies, and capital letters denote spatial Fourier transforms, i.e., the transforms of the blurred and unblurred images are given by the following:

$$B(f_x,f_y) = \int_{-\infty}^{\infty}\int_{-\infty}^{\infty} b(x,y)\, e^{-i2\pi(f_x x + f_y y)}\, dx\, dy$$

$$A(f_x,f_y) = \int_{-\infty}^{\infty}\int_{-\infty}^{\infty} a(x,y)\, e^{-i2\pi(f_x x + f_y y)}\, dx\, dy$$

The system function of the distorting atmosphere is given below:

$$H(f_x,f_y) = \int_{-\infty}^{\infty}\int_{-\infty}^{\infty} h(x,y)\, e^{-i2\pi(f_x x + f_y y)}\, dx\, dy$$

If $H(f_x,f_y)$ is unique and if $A(f_x,f_y)$ has no **zeroes**, then $H(f_x,f_y)$ is found as follows:

$$H(f_x,f_y) = \frac{B(f_x,f_y)}{A(f_x,f_y)}$$

If 0 does not change in space or time, then the original unblurred images may be determined by the following manipulation:

$$a(x,y) = \frac{1}{2\pi}\int_{-\infty}^{\infty}\int_{-\infty}^{\infty} A(f_x,f_y)\, e^{i2\pi(f_x x + f_y y)}\, df_x\, df_y$$

Consider again the satellite cloud prediction problem: Assuming linearity, shift-invariance and the stationarity of the operator 0, the transform of the predictand $C_p(f_x,f_y) = H(f_x,f_y)B(f_x,f_y)$

or

$$C_p(f_x,f_y) = \frac{[B(f_x,f_y)]^2}{A(f_x,f_y)}$$

In the spatial domain

$$c(x,y) = \int_{-\infty}^{\infty}\int_{-\infty}^{\infty} b(\alpha - x, \beta - y)\, h(\alpha,\beta)\, d\alpha\, d\beta$$

The advantage of working in the frequency domain rather than in the spatial domain is that determining $H(f_x,f_y)$ by dividing $B(f_x,f_y)$ by $A(f_x,f_y)$ is much easier than by deconvolving b(x,y) with a(x,y) to find h(x,y).

If the conditions of linearity, shift-invariance, and stationarity of 0 hold, then given continuous functions a(x,y) and b(x,y), one could solve (predict) for $c_p(x,y)$ <u>exactly</u> [$c_p(x,y) = c_v(x,y)$]. However, the atmosphere acts in a shift-varying manner. The expansion of a cloud mass, for example, is a shift-varying operation. The sudden appearance of cirrus blowoff above a cluster of cumulonimbus clouds, a common occurrence in the tropics, is shift-varying also. In addition, the sudden appearance of clouds is a non-linear operation. Towering cumulus cloud structures, growing from clear air, can develop in less than thirty minutes. To make matters worse, one must <u>sample</u> data, thereby obtaining the discrete functions $a(x_i,y_j)$, $b(x_i,y_j)$, rather than the continuous functions a(x,y) and b(x,y). This means that by the sampling theorem (also intuitively) the higher frequency components are at least partially lost because of aliasing.

The space invariance condition has been shown to be not entirely restrictive, (Robbins, 1970). Consider the Mellin transform, $\hat{G}(x)$, of g(x):

$$\hat{G}(s) = \int_0^{\infty} x^{s-1}\, g(x)\, dx$$

letting $x = e^w$,

$$\hat{G}(s) = \int_{-\infty}^{\infty} g(e^w) e^{ws}\, dw$$

setting $s = i\omega$

$$\hat{G}(-i\omega) = \int_{-\infty}^{\infty} g(e^w) e^{-i\omega w}$$

or since $\omega = 2\pi f$

$$\hat{G}(f) = \int_{-\infty}^{\infty} g(e^w)\, e^{-i 2\pi f w}\, dw$$

The latter now expresses $\hat{G}(f)$ as a Fourier transform. Now the Mellin transform has the following useful property:

Consider a one-dimensional system in which g(x) is expanded by a scale factor a. Since the Mellin transform of g is $\hat{G}(s)$, the Mellin transform of g(ax) is $a^{-s}\hat{G}(s)$. The system function $H(S) = \hat{G}(s)$ expanded scale/ $\hat{G}(s)$ original becomes $\frac{a^{-s}\hat{G}(s)}{\hat{G}(s)} = a^{-s}$. The prediction of the third image is obtained first by multiplying the system function by the Mellin transform of the second image, $a^{-s}\ \hat{G}(s)$. So, the Mellin transform of the predicted image is simply the following:

$$\hat{G}_p(s) = a^{-s}\left[a^{-s}\,\hat{G}(s)\right] = a^{-2s}\ \hat{G}(s)$$

The inverse transform of $\hat{G}_p(s)$ is $g(a^2x)$, i.e. the function g(x), whose scale is further scaled by another factor a.

Therefore, one must first distort the original images by setting $x = e^{w_x}$

$$y = e^{w_y}$$

Then one proceeds in the following manner: Divide the two-dimensional Fourier transform of the second image by the two-dimensional Fourier transform of the first image and multiply this by the two-dimensional Fourier transform of the second image. Before inverse transforming, distort the spatial coordinates again by setting $x = e^{w_x}$

$$y = e^{w_y}$$

The primary disadvantage of using the Mellin transform is the change of spatial scale distortion. The points w_x and w_y corresponding to x and y require a sampling rate greater than that of the sampled image.

Another way of solving the problem of shift-varying systems is to separate the system into distinct shift-invariant and shift-varying systems. First solve the problem as though the system were shift-invariant. Then determine the scale factor of expansion or of contraction. Determining the scale factor requires the following property of the Fourier transform:

If $G_1(f)$ is the Fourier tranform of $g(x)$, then $G_2(f)=\frac{G(\frac{f}{a})}{|a|}$ is the Fourier transform of $g(ax)$.

Therefore, the scale factor "a" may be obtained by the following relation, derived from the latter expression:

$$|a| = \left.\frac{G_1(f)}{G_2(f)}\right|_{f=0}$$

For a two-dimensional image one must seek two scale factors, one each for the x and y directions. One must now find a compromise between the two scale factors and the system function $H(f_x,f_y)$.

One is now in the position of formulating a prediction equation. If the system is linear and shift-invariant and consists of discrete (sampled) data, one can use the following equations:

letting $A(f_{x_i},f_{y_j}) = |A|e^{i\theta_A(f_{x_i},f_{y_j})}$

$$B(f_{x_i},f_{y_j}) = |B|e^{i\theta_B(f_{x_i},f_{y_j})}$$

$$C_p(f_{x_i},f_{y_j}) = |C_p|e^{i\theta_C(f_{x_i},f_{y_j})}$$

$$\ln|C_p| = \ln|B| + \ln|B| - \ln|A|$$
$$= \ln|B| + \ln|H|$$

and,

angle of $C_p(f_{x_i}, f_{y_j})$ = 2[angle of $B(f_{x_i}, f_{y_j})$] − angle of $A(f_{x_i}, f_{y_j})$

The phase angle is found by a linear prediction equation while the amplitude is found via a non-linear prediction equation. One can now modify the prediction equation in order to correct errors made in assuming linearity. The prediction equation can be written as the following:

$$\ln\left|C_p(f_{x_i}, f_{y_j})\right| = \ln\left|B(f_{x_i}, f_{y_j})\right| + K\left[\ln|B(f_{x_i}, f_{y_j}| - \ln|A(f_{x_i}, f_{y_j}|\right]$$

The angle equation remains unchanged (see Figure 1) where K is a real constant.

If K = 1, one is predicting by linear extrapolation, the phase and amplitude of the transform.

If K = 0, one is keeping the amplitude constant with time, but is predicting by linear extrapolation the phase angle. Since a phase shift in the frequency domain corresponds to spatial shift in the space domain, one is in effect (K=0) predicting motion of the gross features of the cloud pattern but not significant changes in the intensity of the cloud pattern.

An intensifying cloud mass (i.e. one increasing in brightness) may be expressed as the constructive interference of two or more travelling waves. Conversely, a weakening cloud mass (i.e. one decreasing in brightness) may be expressed as the destructive interference of two or more travelling waves. This is the only way cloud masses for the K=0 prediction

can intensify. For K=1, this interference is augmented or diminished by amplification of spectral components.

Procedure

Before working with actual satellite data, I experimented with idealized shapes in order to test out the prediction scheme on a perfectly predictable system. A useful shape is the circle, since it is simple and somewhat like real cloud patterns. I first synthesized a filled-in circle of uniform brightness as image $a(x_i,y_j)$, and an identical circle displaced as $b(x_i,y_j)$, (i.e. 0 is a simple linear displacement operator), where

$$b(x_i, y_j) = a(x_i - \alpha, y_j - \beta) \qquad \begin{matrix} 0 \le i \le 63 \\ 0 \le j \le 63 \end{matrix}$$

where α and β are the x and y displacements. Taking the discrete Fourier transforms of a and b,

$$A(f_{x_i}, f_{y_j}) = \sum_{i=0}^{63} \sum_{j=0}^{63} a(x_i, x_j)\, e^{-i\frac{2\pi}{64}(f_{x_i} X_i + f_{y_j} Y_j)}$$

$$B(f_{x_i}, f_{y_j}) = \sum_{i=0}^{63} \sum_{j=0}^{63} b(x_i, y_j)\, e^{-i\frac{2\pi}{64}(f_{x_i} X_i + f_{y_j} Y_j)}$$

$$= A(f_{x_i}, f_{y_j})\, e^{-j\frac{2\pi}{64}(f_{x_i}\alpha + f_{y_j}\beta)}$$

so,

the system function

$$H(f_{x_i}, f_{y_j}) = \frac{B(f_{x_i}, f_{y_j})}{A(f_{x_i}, f_{y_j})} = e^{-i\frac{2\pi}{64}(f_{x_i}\alpha + f_{y_j}\beta)}$$

therefore,

$$C_p(f_{x_i}, f_{y_j}) = e^{-i\frac{2\pi}{64}(f_{x_i}\alpha + f_{y_j}\beta)}\, B(f_{x_i}, f_{y_j})$$

and,

$$c_p(x_i, y_j) = \frac{1}{4096} \sum_{i=0}^{63} \sum_{j=0}^{63} C(f_{x_i}, f_{y_j})\, e^{i\frac{2\pi}{64}(f_{x_i} X_i + f_{y_j} Y_j)}$$

This simple exercise illustrates only that a certain class of systems (simple linear motion) is perfectly predictable by this method and has a simple prediction formula.

It must be mentioned that the 2-dimensional Fourier transform is periodic in f_x and in f_y, i.e.

$$A(f_x, f_y) = A(f_x \pm 2\pi, f_y) = A(f_x, f_y \pm 2\pi) = A(f_x \pm 2\pi, f_y \pm 2\pi)$$

When considering the transforms, I therefore can restrict myself to one rectangular box $0 \leq f_x \leq 2\pi$ and $0 \leq f_y \leq 2\pi$.

Since $c_p(x_i, y_j)$ is a discrete matrix of points, it may also be expressed as the circular convolution of $h(x_i, y_j)$ with $b(x_i, y_j)$ (Gold and Rader, 1969), that is by the following expression:

$$c_p(x_i, y_j) = \sum_{\gamma_i=0}^{63} \sum_{\gamma_j=0}^{63} h(\gamma_i, \gamma_j)\, b\left[((\gamma_i - x_i)), ((\gamma_j - y_j))\right]$$

where $((q))$ denotes q modulo 64

This expression is in contrast to the "simple" convolution expression of continuous systems. In effect, points on the border of an image may affect the opposite border of the next image; e.g. linear motion in the west-east direction, if sufficiently large will force a shape to leave the western edge and reappear at the eastern side of the image. One would suspect, therefore, that in addition to the reduced accuracy of predictions related to missing all the data points (i.e. using sampled functions), one would also expect higher errors at the boundaries of the image.

Returning now to the ideal circle, I then let $a(x_i, y_j)$ be a circle and $b(x_i, y_j) = a(\alpha x_i, \beta y_j)$, that is, 0 is a changing of spatial scale. The scale factor appears as the following:

$$\left|\alpha\,\beta\right| = \left.\frac{B(f_{x_i}, f_{y_j})}{B\left(\frac{f_{x_i}}{\alpha}, \frac{f_{y_j}}{\beta}\right)}\right|_{f_{x_i} = f_{y_j} = 0}$$

I determined α and β separately by iteration, i.e. by starting with an α_0, letting $\beta_0 = \frac{|\alpha\beta|}{\alpha_0}$, and minimizing the following expression increasing α_0 at each step of the procedure:

$$E = \sum_{i=0}^{63} \sum_{j=0}^{63} \left| a(\alpha_0 x_i, \beta_0 y_j) - b(x_i, y_j) \right|$$

For my ideal circle, α and β converged to the correct scale factors.

One could then combine the two former processes to provide a method which predicts linear motion and scale change, i.e. a linear shift-invariant change and a linear shift-varying change. The scale change would be made to the already shifted predicted image. However, after having carefully examined many satellite cloud patterns, I reached the conclusion that finding a unique scale factor for sequences of images would be nearly impossible, since the cloud shapes are so complex, and because some shapes within the image may expand while others remain fixed.

I therefore decided to restrict myself to the prediction of satellite cloud patterns using the following relation:

$$\ln\left|C_p(f_{x_i}, f_{y_j})\right| = \ln\left|B(f_{x_i}, f_{y_j})\right| + K\left[\ln\left|B(f_{x_i}, f_{y_j})\right| - \ln\left|A(f_{x_i}, f_{y_j})\right|\right]$$

$$\text{angle of } C_p(f_{x_i}, f_{y_j}) = 2\left[\text{angle of } B(f_{x_i}, f_{y_j})\right] - \text{angle of } A(f_{x_i}, f_{y_j})$$

where K is a constant explained earlier.

My first task was the selection of data. NESS (National Environmental Satellite Service) was unable to supply satellite tapes from the ATS-III

satellite, which is in geosynchronous orbit over the Atlantic. This was unfortunate, since I have had some experience in identifying cloud systems over the Atlantic. NESS was later able to supply tapes for 15 August 1971 from the ATS-I satellite which is in geosynchronous orbit over the Pacific (2°N 149°W).

I first examined rather closely a series (Table 1) of full Earth gridded prints. Numerous frontal structures (west of California and west of 180°W x 40°N, for example) were apparent, but their prediction probably would not be very rewarding, since the frontal cloud mass is only a "simple" moving strip of cloud mass. An apparent tropical cyclone (120°Wx 25°N) was somewhat obscured by stratus to the north off the coast of Southern California and by what is probably stratocumulus to the west of the circulation. I therefore selected a feature, probably associated with a tropical wave whose axis is approximately N-S about 165°W, and whose horizontal E-W extent is from 155°W to 170°W. The northern region of the feature is characterized by an "inverted-V" shaped structure of cloud bands, similar to those seen in the Atlantic (Frank, 1969). The clouds associated with this apparent disturbance extend southeastward and southwestward into the Intertropical Convergence Zone at about 7-8°N. The N-S extent of this feature is approximately from the bottom of the ITC at 5°N to about 20°N.

I then more closely inspected the cloud mass by looking at a sequence of mercator mapped photographs from 105°W to 170°E and from 30°S to 40°N. Within the area of the system from 15°N to 5°N there are numerous banded structures. The eastern edge (163°W to 170°W) of the disturbance is characterized by a complex mass of smaller bands and cirrus outflowing toward

the southeast, indicating a strong upper trospheric wind from the northwest.

The eastern region (from about 163°W to 158°W) is characterized by three parallel cloud masses aligned roughly ENE to WSW. The top band is quite solid in comparison to the other two and shows strong cirrus outflow. The bottom two are aligned more W-E than the top bands, but only slightly more. They, however, look more cellular or grainy and less solid. I would conjecture that they consist primarily of cumulus congestus towers whose tops have not yet reached the outflow layer. It is quite remarkable that the upper band which obviously consists of cumulonimbus complexes has a quite similar structure to the other bands. Perhaps the presence or absence of cirrus is not all that important. The dynamic processes occurring within the disturbance can only be surmised, since meteorological data in the area is extremely sparse. The closest surface observation station to the disturbance is Johnston Island at 169.6°W, 17°N. Its observations from 0000Z August 15, 1971 to 1800Z August 15, 1971 indicate the presence of towering cumulus clouds; a rainshower occurred sometime between 12Z and 18Z. The meteorological observations for four time periods are given in Table 2. This station is in a region north of most of the cumulonimbus activity. It is located just south of a band aligned NE-SW associated with the "inverted-V" structure. I concluded that the band was moving westward, and probably passed by the station with showers sometime before local sunrise. I finally decided to choose the region bounded by 5°N to 15°N and 165°W to 155°W, a square of approximately 1000 km by 1000 km. The three parallel cloud masses aligned ENE to WSW described earlier show a distinct westward motion and slight change in character, i.e. shape and alignment, over the period from 1809Z to 2208Z. According to a recent classification the cloud patterns are of the cloud cluster scale (Sikdar

and Suomi, 1971).

I therefore obtained three digitized mercator mapped satellite tapes for 1809Z, 2008Z and 2208Z. They represent three sequences of images, each separated by about Δt = two hours. This Δt, as far as I could tell, was a good time interval to choose, since features of this space scale seem to change nearly unnoticeably for Δt on the order of twenty-four minutes, the period with which actual satellite data is gathered; however, features of this space scale do change dramatically over a period of one day. In fact, the wave is barely noticeable at all on the satellite photographs of 14 August 1971 or on 16 August 1971. This ephemeral characteristic is quite similar to that of Atlantic disturbances.

I therefore let $a(x,y)$ be the photograph at 1809Z (Figure 2)

$b(x,y)$ be the photograph at 2008Z (Figure 3)

$c_v(x,y)$ be the photograph at 2208Z (Figure 4)

Each image could be at most a square array of 256 x 256 points quantized from 0 to 63(64 levels), 0 representing the darkest level and 63 representing the brightest level. Each array is only a small portion of the tape, which actually contains data from 170°E to 105°E and from 40°S to 40°N. The horizontal resolution of the picture is approximately 2 1/2 nautical miles near the equator. In order to fit the three cloud bands into one smaller 128 x 128 array, I sampled the image every five nautical miles, thus reducing the number of grid points by a factor of four.

I then had to normalize the contrast of the three images. Contrast and illumination vary as a function of solar angle, and hence the 1809Z image near sunrise does not have very much contrast and appears somewhat washed out, relative to the 2208Z image of near local noon. I adjusted

the contrast and intensity by comparing the printouts of a(x,y), b(x,y) and $c_v(x,y)$ point by point, taking pains to compare the more intense region of cloud bands with the darker cloudless regions. The contrast and intensity of the three images was normalized according to the following relations:

$$a(x,y) \longrightarrow \begin{cases} a(x,y) + 9 & a(x,y) < 20 \\ a(x,y) + 5 & a(x,y) \geq 20 \end{cases}$$

$$b(x,y) \longrightarrow b(x,y) + 4$$

$c_v(x,y)$ remains unchanged

The success of this normalization was judged subjectively (Figures 5,6,7).

In addition to the actual printout of grid **point** intensities, I also printed out simulated gray scale photographs. The three images were converted into two-dimensional discrete Fourier transforms $A(f_{x_i}, f_{y_j})$, $B(f_{x_i}, f_{y_j})$, $C(f_{x_i}, f_{y_j})$. Each two-dimensional transform was then low-pass filtered. The low pass filter was a circular cutoff filter, i.e. no portion of the two-dimensional spectrum at a radius of greater than $\frac{6}{128}(2\pi)$ cycles/mile (i.e. no wavelengths greater than one-sixth of the width of the picture) was allowed to pass:

$$\left| H_{filter}(f_{x_i}, f_{y_j}) \right| = \begin{cases} 1 & (f_{x_i} + f_{y_j})^{\frac{1}{2}} \leq \frac{6}{128}(2\pi) \\ 0 & (f_{x_i} + f_{y_j})^{\frac{1}{2}} > \frac{6}{128}(2\pi) \end{cases}$$

This cutoff frequency, $\frac{6}{128}(2\pi)$ cycles/mile, was chosen because most of the picture's energy is confined to lower frequencies. I did not experiment with other filters having different cutoff frequencies because of the large expense involved in two-dimensional Fourier transforming via computer.

The filtered images $a(x_i,y_j)$ (Fig. 5), $b(x_i,y_j)$ (Fig. 6), and $c(x_i,y_j)$ (Fig. 7), i.e. the inverse transformed filtered transforms of $A(f_{x_i},f_{y_j})$, $B(f_{x_i},f_{y_j})$ and $C_v(f_{x_i},f_{y_j})$ look like smoothed versions of the original images. However, they still retain the essential gross features of the unfiltered images. The higher frequency features such as small individual cumulonimbus towers and meso-convective scale regions (Sikdar and Suomi, 1971) are obscured. This is desirable, however, in a scheme in which a two-hour prediction is made of phenomena characterized by horizontal scales from one to ten kilometers down to cumulus tower size, and characterized by time scales of twenty minutes. The filtering in effect cuts out these small scale components of the image that possess little predictability, and therefore may be regarded as high frequency noise. If the noise (i.e. all high frequency components) were left in the picture, it is probable that some high frequency components would be excessively and unrealistically amplified to the point where the images would be blanketed by noise. A crude study this summer in which the cutoff frequency of the filter was varied (Bluestein, 1971) demonstrated quite clearly that the predicted image is totally obscured in noise as the cutoff frequency is increased beyond a certain radius of spatial frequency.

The filtered components were then stored on cards for the remainder of the project. $C_p(f_{x_i},f_{y_j})$ was predicted from the filtered $A(f_{x_i},f_{y_j})$ and $B(f_{x_i},f_{y_j})$ for K=1 and for K=0. The final predicted images $c_p(x_i,y_j)$ (Fig. 8) were printed for comparison with the observed image, while $C_p(f_{x_i},f_{y_j})$ was stored on cards for error analysis.

Results

The resulting images $c_p(x_i,y_j)$ (Fig. 8) are compared to the actual filtered $C_v(x_i,y_j)$ (Fig. 7) for 2208Z. $c_p(x_i,y_j)$ with K=1 appears to have diagonal ripples oriented along a NE to SW direction. These ripples are a result of very large spectral components

$$\left[+2\left(\frac{2\pi}{128}\right), -2\left(\frac{2\pi}{128}\right)\right] \text{ and } \left[-2\left(\frac{2\pi}{128}\right), +2\left(\frac{2\pi}{128}\right)\right]$$

which sinusoidally modulate the image along the axis perpendicular to the line between them. The large increase in spectral component amplitude of these two points in the transform is a result of overamplification of the filtered $B(f_{x_i},f_{y_j})$. $c_p(x_i,y_j)$ with K=0 appears unrippled. In effect, no amplification of the filtered $\left|B(f_{x_i},f_{y_j})\right|$ was allowed.

These are simple subjective evaluations. One much more objective way of evaluating the results is to compare the error of the forecast to "standard" forecasts such as "climatology" and "persistence". The error E of a forecast for a 128 x 128 point array is defined as the following:

$$E = \frac{1}{16384} \sum_{i=0}^{127} \sum_{j=0}^{127} \left[\left(f(x_i,y_j) - o(x_i,y_j)\right]^2\right.$$

where $f(x_i,y_j)$ is the forecasted image and

$o(x_i,y_j)$ is the observed image.

Now, letting $F(f_{x_i},f_{y_j})$ and $O(f_{x_i},f_{y_j})$ be the two-dimensional discrete Fourier transforms of $f(x_i,y_j)$ and $o(x_i,y_j)$ respectively, then,

$$f(x_k,y_\ell) - o(x_k,y_\ell) = \frac{1}{16384} \sum_{i=0}^{127} \sum_{j=0}^{127} \left[F(f_{x_i},f_{y_j}) - O(f_{x_i},f_{y_j})\right] e^{i\frac{2\pi}{128}(f_{x_i}x_k + f_{y_j}y_\ell)}$$

therefore,

$$E = \left(\frac{1}{16384}\right)^2 \sum_{i=0}^{127} \sum_{j=0}^{127} \left|F(f_{x_i},f_{y_j}) - O(f_{x_i},f_{y_j})\right|^2$$

$$E = \left(\frac{1}{16384}\right)^2 \sum_{i=0}^{127}\sum_{j=0}^{127} \left[\left(\mathrm{Re}\, F(f_{x_i}, f_{y_j}) - \mathrm{Re}\, O(f_{x_i}, f_{y_j})\right)^2 + \left(\mathrm{Im}\, F(f_{x_i}, f_{y_j}) - \mathrm{Im}\, O(f_{x_i}, f_{y_j})\right)^2\right]$$

In this way, the error E can be evaluated directly in the frequency domain (via a form of Parseval's theorem) by taking the square of 169 differences, rather than in the filtered spatial domain by taking the square of 16,384 differences.

Now, "climatology" is defined as a set of image points, each of which equals the time averaged (denoted by) brightness of that point on Earth. "Climatology", however, is assumed to be the same at each point because the space scale of the image is small.

$$f_{\text{climatology}}(x_i, y_j) = \overline{f(x_i, y_j)} = \frac{1}{16384}\sum_{i=0}^{127}\sum_{j=0}^{127} f(x_i, y_j) \cong \frac{1}{16384}\frac{\left[A(0,0) + B(0,0) + C_v(0,0)\right]}{3}$$

or equivalently,

$$F_{\text{climatology}}(f_{x_i}, f_{y_j}) = \begin{cases} \frac{1}{16384}\cdot\frac{\left[A(0,0) + B(0,0) + C_v(0,0)\right]}{3} & f_{x_i} = f_{y_j} = 0 \\ 0 & \text{elsewhere} \end{cases}$$

"Persistence" is defined as a forecast of no change, that is, the forecast is the past state:

$$f_{\text{persistence}}(x_i, y_j) = b(x_i, y_j)$$

or equivalently,

$$F_{\text{persistence}}(f_{x_i}, f_{y_j}) = B(f_{x_i}, f_{y_j})$$

From these definitions, one would expect climatology to be a poor two-hour forecast, since "persistence" is good. "Persistence" would probably be a good forecast, since the actual gross features of the cloud pattern don't change a great deal over a two-hour period.

The results confirm this suspicion (Table 3). The error of the predicted picture with K=1 is higher than both that of "climatology" and "persistence" due to the ripples. The error of the predicted picture with K=0 is lower than that of "climatology", but is slightly more than that of "persistence". Evidently, "climatology" can be "beaten" using this scheme by predicting only the transform's phases and by keeping the transform's amplitudes constant with time or by using "persistence", which is cheaper. "Persistence", however, is hard to "beat" using this scheme. While computing the errors in the mean square sense provides some objective way of evaluating the degree of success attained by the predictions scheme, one can also make simple measurements of prominent features and their changes directly from the images. One test is to compare the actual speed of the three cloud bands with (1) the predicted speed of each cloud band, (2) the predicted phase speed of the image as a whole and (3) the climatological speeds usually attained by these tropical waves (not the same as "climatology", which has zero phase speed). While the actual and predicted speeds are measured directly, the phase speed can be determined by expressing the image as a sum of travelling waves.

let $\mathcal{L}(\vec{r}, \vec{v}, t) = \mathcal{L}(x_i, y_j)\, e^{i(\omega_{x_i} x_i + \omega_{y_j} y_j - \omega_{x_i} v_{x_i} t - \omega_{y_j} v_{y_j} t)}$

where $\mathcal{L}$ is the image at time t

$\vec{r}$ is the position vector

$\vec{V}$ is the phase velocity vector of the pattern

$\omega = 2\pi f$

At a given point in the spatial domain the change in phase ($\Delta\phi$)during a time interval Δt , is given by the product of Δt with the dot product of the angular frequency vector and the velocity vector.

$$\Delta\phi(\omega_x, \omega_y) = (\vec{\omega}\cdot\vec{V})\Delta t = (\omega_x V_x + \omega_y V_y)\Delta t$$

or

$$\Delta\phi(f_x, f_y) = 2\pi\Delta t(f_x V_x + f_y V_y)$$

So,

$$\Delta\phi(f_x,f_y) = \tan^{-1}\frac{Im[B(f_x,f_y)]}{Re[B(f_x,f_y)]} - \tan^{-1}\frac{Im[A(f_x,f_y)]}{Re[A(f_x,f_y)]} = (2\pi)(2)[f_x V_x + f_y V_y]$$

f_x, f_y are measured in cycles/nautical mile,

V_x, V_y are measured in knots.

Along the f_y axis, $f_x = 0$, and V_y can be found as a function of f_y. Along the f_x axis, $f_y = 0$ and V_x can be found as a function of f_x. Elsewhere in the frequency domain, a different V_x and V_y will be found. (There is some freedom in defining V_x and V_y; one might remove this freedom by restricting V to be normal to the cloud mass.) The average phase velocities V_x and V_y might give some indication of the average gross motion of the cloud patterns. If the sequence of images consisted of simple displaced cloud masses, then V_x and V_y would be the same everywhere. Since the real images comprise a shift-varying system, there will be some phase distortion, i.e. V_x and V_y will vary as a function of spatial frequency or equivalently,

the phase will vary nonlinearly as a function of spatial frequency. In other words, low frequencies will "move" at different "speeds" than high frequencies. This dispersion effect is perhaps analogous to that associated with one-dimensional wave-like equations.

Calculations of V_x and V_y via the previous method is very difficult in practice, since the angles ϕ are measured modulo 2π . Therefore, in calculating $\Delta\phi$, one might encounter errors in multiples of 2π . V_x and V_y would therefore be correspondingly under or over-estimated. Another method of calculating V_x and V_y, which is not restricted to angles only along the f_x and f_y axis, is the following:

Calculate the gradient of $\Delta\phi = \vec{\nabla}[\Delta\phi(\omega_x, \omega_y)] = \frac{\partial \Delta\phi}{\partial x}\vec{\imath}_x + \frac{\partial \Delta\phi}{\partial y}\vec{\imath}_y$ where $\vec{\imath}_x$ is the unit vector pointing toward the east and $\vec{\imath}_y$ is the unit vector pointing towards the north.

$$\vec{\nabla}(\Delta\phi) = \Delta t\left[V_x \vec{\imath}_x + V_y \vec{\imath}_y\right]$$

V_x is therefore the x derivative of $\Delta\phi$ divided by Δt , and V_y is the y derivative of $\Delta\phi$ divided by Δt . The problem of miscalculating $\Delta\phi$ by multiples of 2π still remains, but V_x and V_y can be found for more points.

It is found that phase speeds vary markedly for the three cloud bands (Table 4), indicating that there is quite a bit of phase distortion. The average computed phase velocities, however are about the same as the climatological velocity (again, <u>not</u> the velocity of the "climatology" forecast which is zero). The measured velocities were obtained by noting the two-hour displacements of the centers of mass of the three cloud bands associated with the filtered images $a(x_i, y_j)$, $b'(x_i, y_j)$ and $c_v(x_i, y_j)$. The

very large westward velocities associated with the lower cloud band which were computed from the actual data (A to B and B to C) may be the result of redevelopment to the west of the original cloud cluster. This is a result of non-advective cloud motion.

Conclusions and Suggestions for Future Work

The results indicate that predictions of phase only, keeping the amplitude of the transformed image constant, are superior to predictions of phase and amplitude. This is due to spurious amplification of certain spectral components, which is manifested by ripples in the spatial domain. However, the "persistence" forecast is still the best forecast.

Other possible error sources may be classified and corrected as the following:

Due to the circular convolution in the spatial domain, clouds tend to move across edges and reappear at the opposite boundary of the image. Errors from this source appear to be minimal, because not much extra cloud material seems to be added at the boundaries of the picture. If this effect were detrimental, one could set the boundaries of the images to zero and consider only what occurs near the center. This is equivalent to multiplying the image by a "window" or "grace" function (Anuta, 1970). For the case in which clouds move primarily in the east-west direction, one does not need to set all borders to zero, but rather only the eastern and western borders to zero.

Due to changes in image contrast, I made subjective corrections. A more objective way of adjusting the contrast is to find the contrast function $f_{\text{contrast}} = \alpha\, a(x_i, y_j) + \beta$ which minimize E, the root-mean-square deviation of the image from "persistence". α and β are found by

solving the simultaneous linear equations which result from the expressions that set the derivative of E with respect to α and β to zero. The importance of correct contrast adjustments must be emphasized: The difference in illumination due to varying solar position may be unrelated to the degree of cloud density or thickness or convection. An increase in solar angle, for example, might suddenly cause tall isolated cumulonimbus towers to appear much brighter. This results in an increase in the high frequency portion of the spectrum and could lead to spurious increases in the high frequency spectral components. This could possibly explain why the K=1 prediction was so poor.

One reason why "persistence" is such a good forecast, is that in this region of the tropics, tropical waves consistently move westward at about the same speed and with about the same period of four or five days. The displacement of a disturbance is small during a forecast period. Spectral studies (Sikdar and Suomi, 1971) and time-longitude sections of tropical cloudiness (Wallace, 1970) during the northern summer confirm this. My forecast, in effect, is a "persistence of phase speed". Perhaps a forecast of "persistence of climatological speed" would be even better. What is not so persistent is the differing modes of convection present in the disturbances. This suggests that perhaps predictions of cloud patterns spaced at twenty-four minutes, keeping all (i.e. not just every other point) the image information, may improve the predictability of the cloud patterns.

Another possible source of error in predicting motions lies in the inaccuracy of the satellite mapping. The images used come from a set

from which some pictures have errors in positioning of less than five miles. Lack of time precludes a regional check on the mapping accuracy of these pictures. A standard landmark, such as Hawaii, however, does seem to remain in the same position in this series. This error source is therefore probably not very significant.

My selection of a spatial cutoff frequency was not chosen to maximize the predictability of this scheme. A study of the effects of various filters on the images might suggest what is an optimal filter. For example, a low-pass filter with a slow rolloff might still keep unwanted noise down at a low level and yet increase the predictability of some higher frequency components.

One would expect the reduction in variance to decrease as the frequency increases. My data show no clear monotonic decrease as a function of frequency. Since I considered only very low frequencies, it is possible that the reduction in variance fluctuates so wildly that a trend is not evident. The trend of reduction in variance perhaps might start to decrease at higher frequencies which I filtered out.

Although the results of the forecast were not too successful, one cannot conclude that the prediction method using transforms is poor, since only one case was treated. It is doubtful, then, that much speculation regarding performance would be meaningful.

Picture Processing Programs

All two-dimensional discrete Fourier transforms and inverse transforms were done via the fast-Fourier transform algorithm (Gold and Rader, 1969) in subroutine HARM of the Scientific Subroutine Package of Fortran IV. My

subroutines FTR and IFTR did the transforming and inverse transforming. GRAYMP is a subroutine designed to simulate a real photograph by combining characters of varying areas and by overprinting characters to create the illusion of a gray scale. MAX is a subroutine which searches for the point which has the maximum amplitude. The PPRINT subroutine prints out the actual intensity values of the elements of the images. FTRH computes $H(f_{x_i},f_{y_j})$ by performing the complex division of $B(f_{x_i},f_{y_j})$ by $A(f_{x_i},f_{y_j})$. FTRC performs the complex multiplication of $H(f_{x_i},f_{y_j})$ with $B(f_{x_i},f_{y_j})$ to compute $C_p(f_{x_i},f_{y_j})$. Subroutine LOOK prints out the real part, imaginary part, and magnitude of a transform that is low-pass filtered, with a cutoff frequency of $\frac{6}{128} \times 2\pi$ cycles/mile. TAPE extracts the selected bits of data from the tape and converts the numbers to a format compatible with the IBM 370 FORTRAN IV processor.

BLOCK DIAGRAM OF FORECAST PROCESS

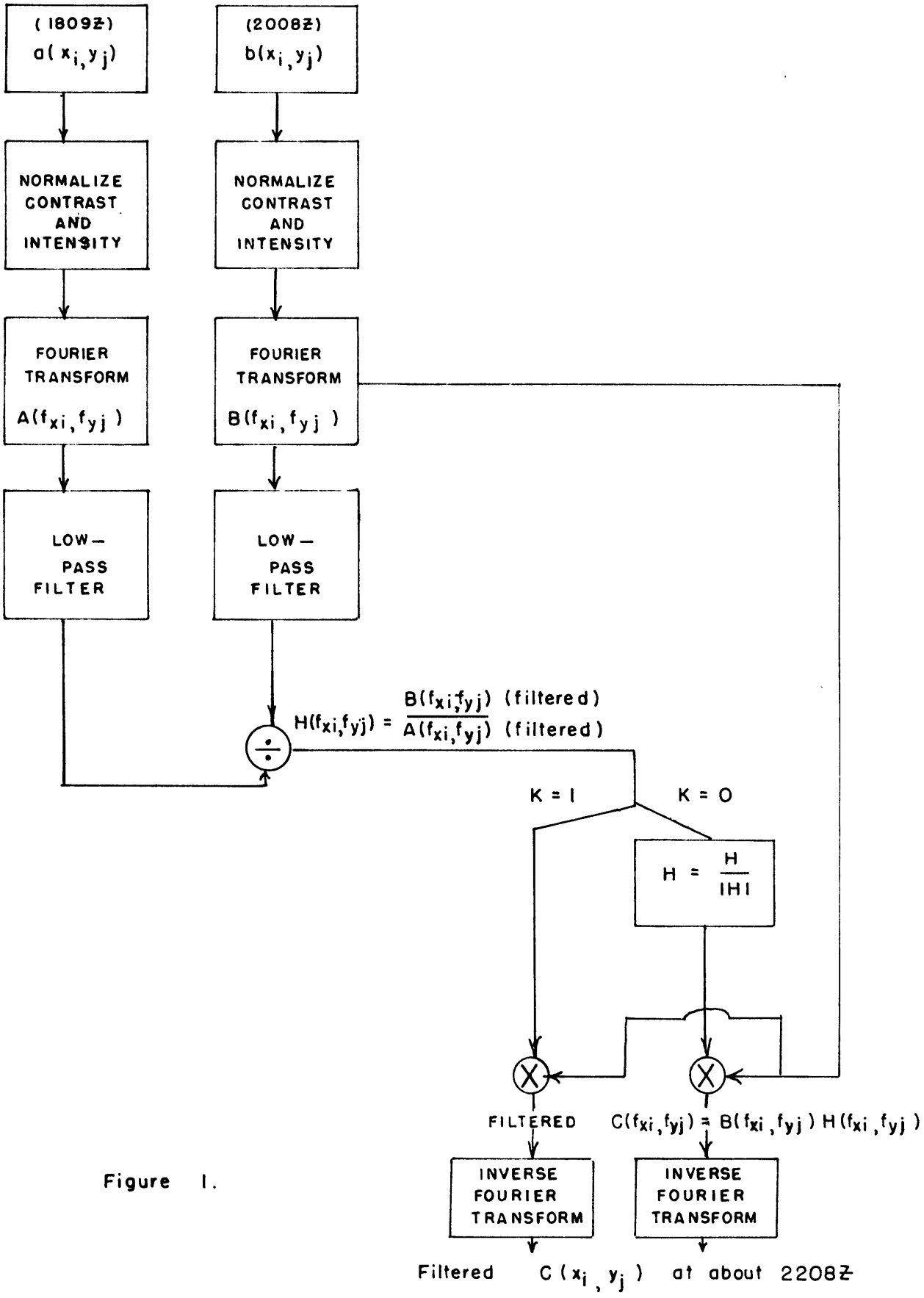

Figure 1.

ORIGINAL MERCATOR-MAPPED 1809Z PHOTOGRAPH

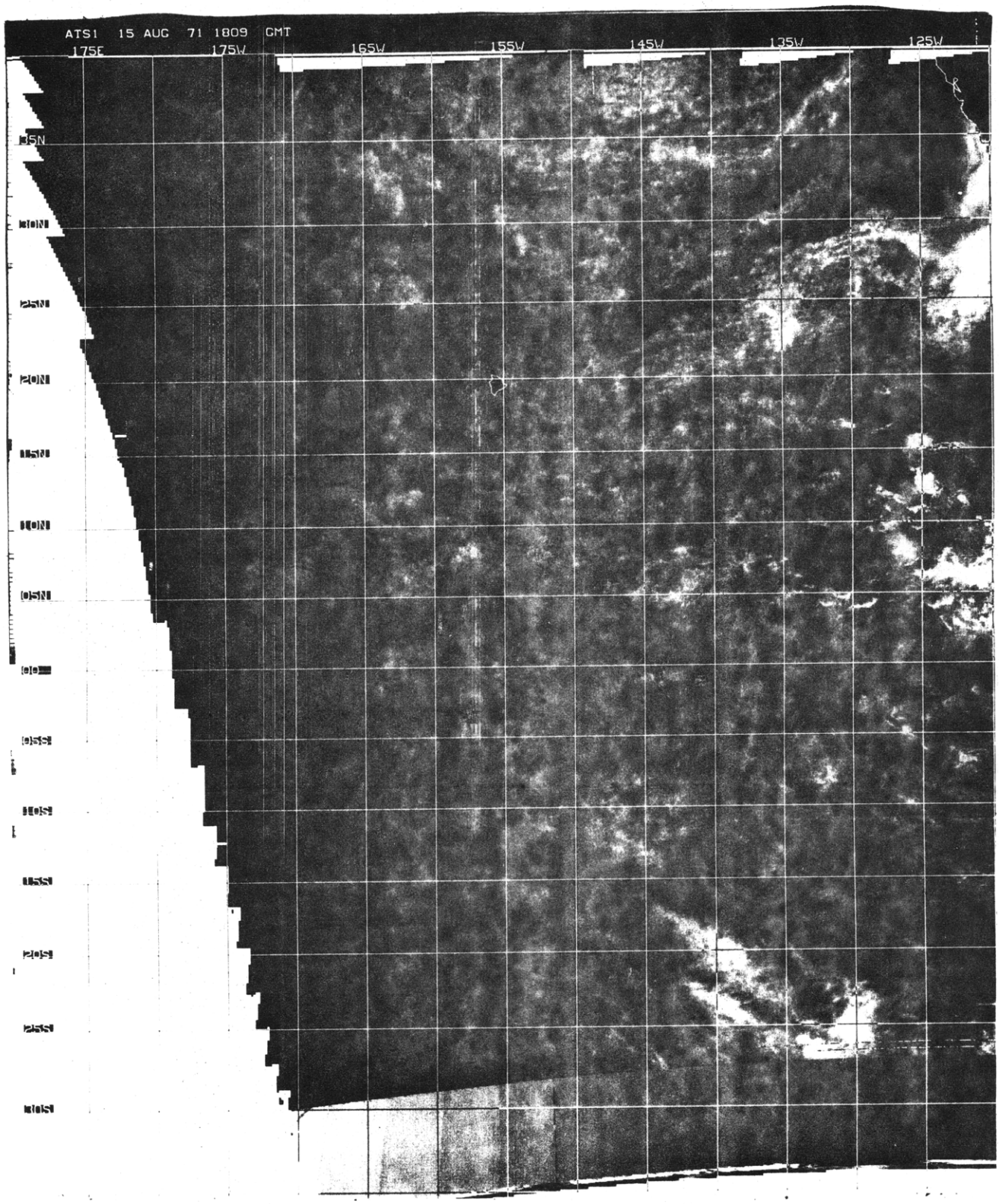

Figure 2

ORIGINAL MERCATOR-MAPPED 2008Z PHOTOGRAPH

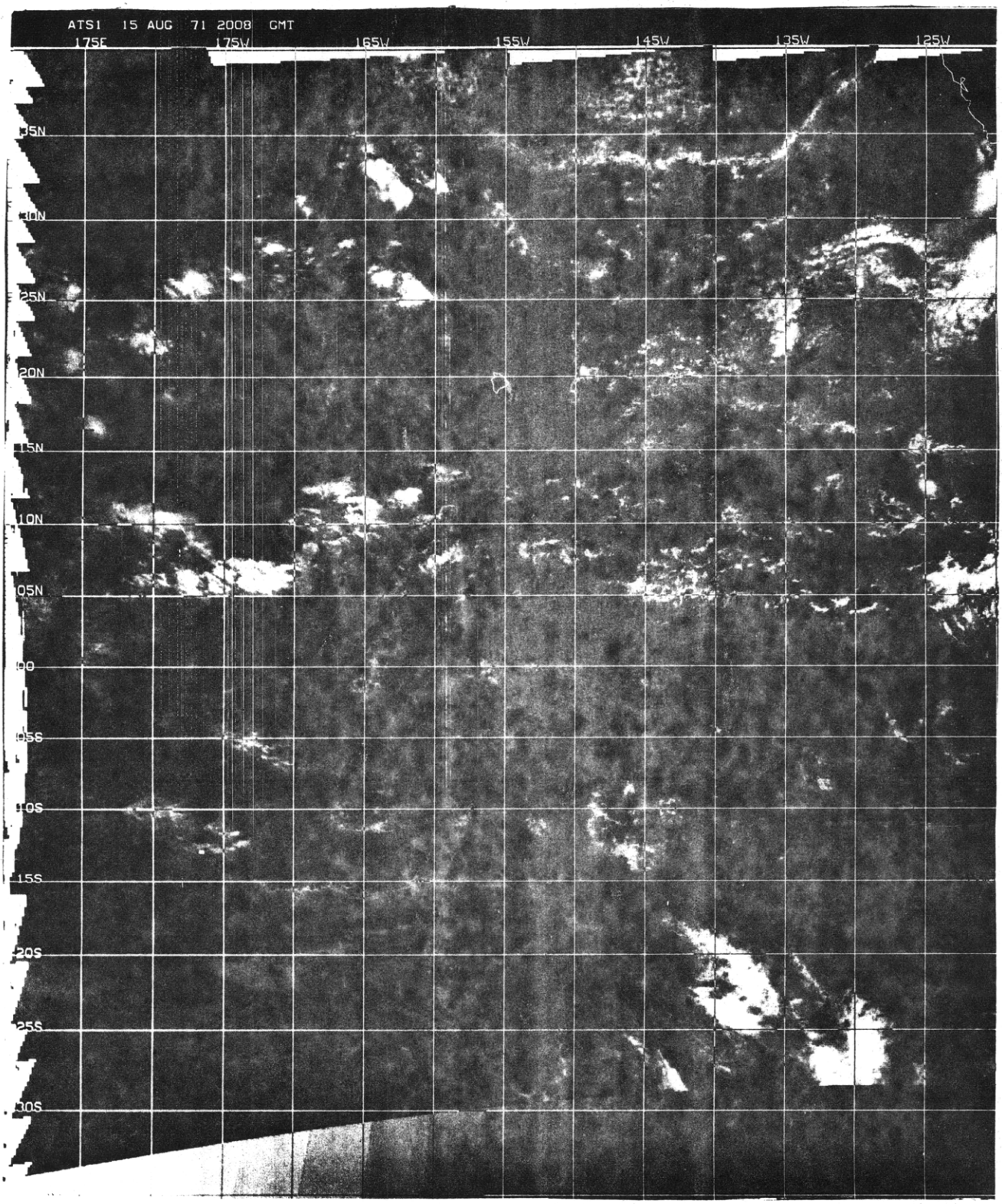

Figure 3

ORIGINAL MERCATOR-MAPPED 2208Z PHOTOGRAPH

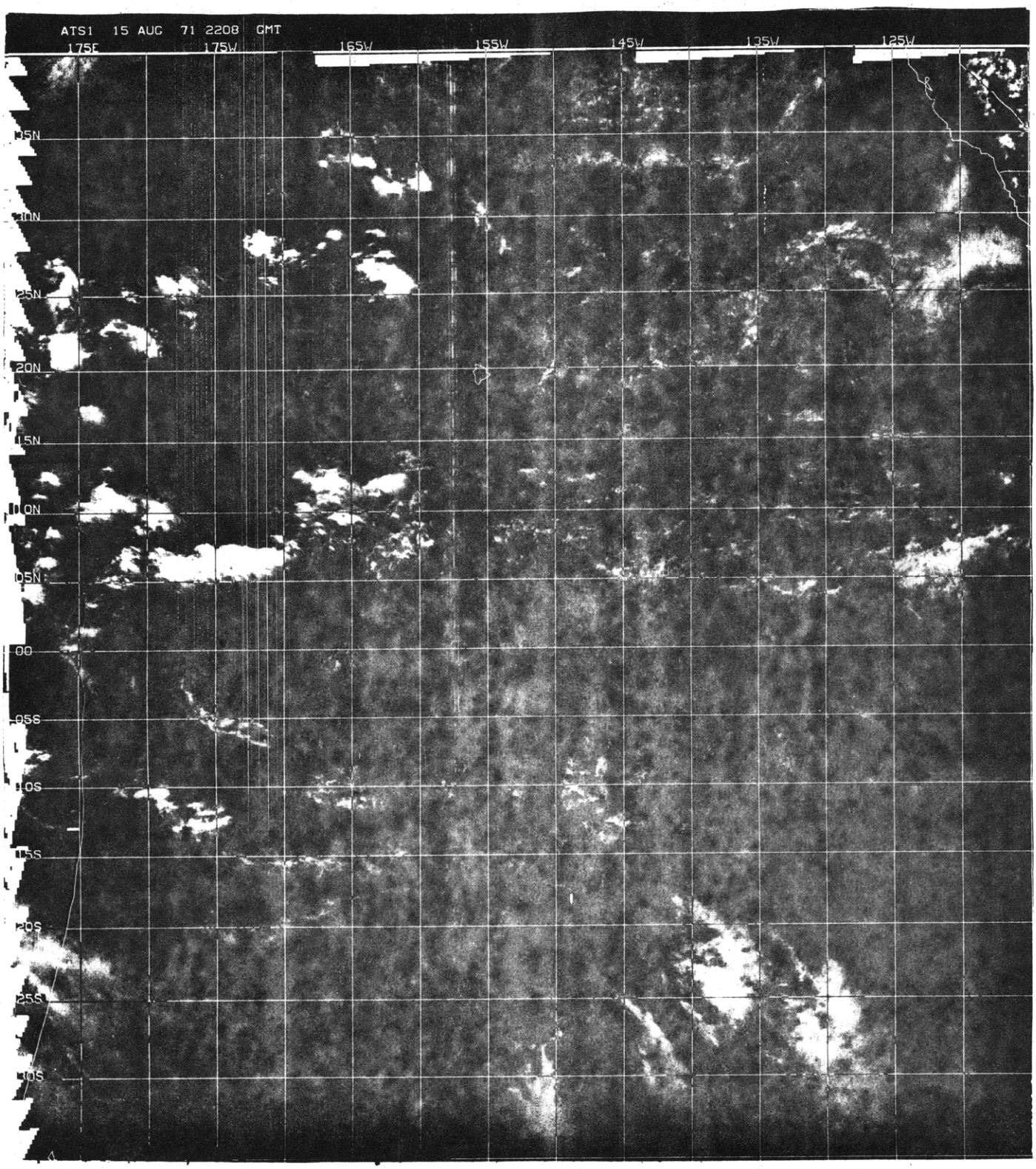

Figure 4

1809Z

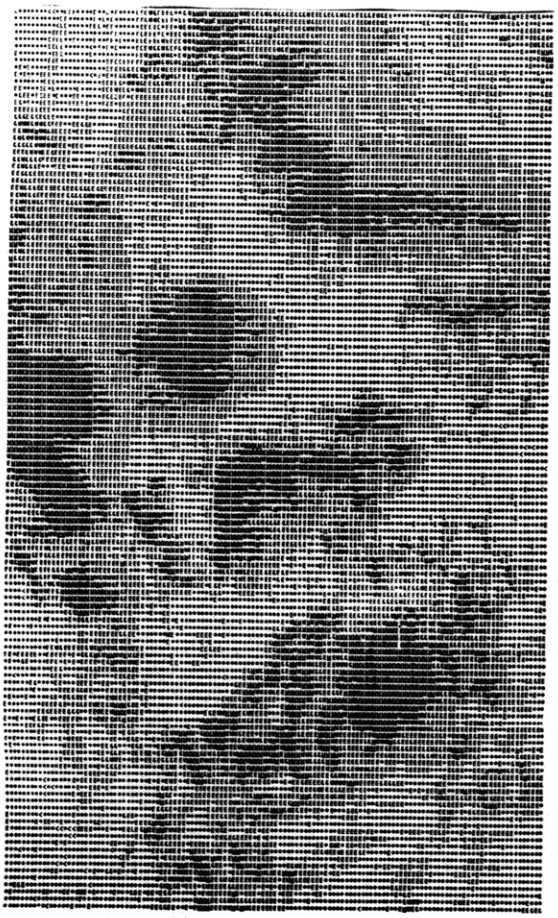

a(x,y)

(normalized)

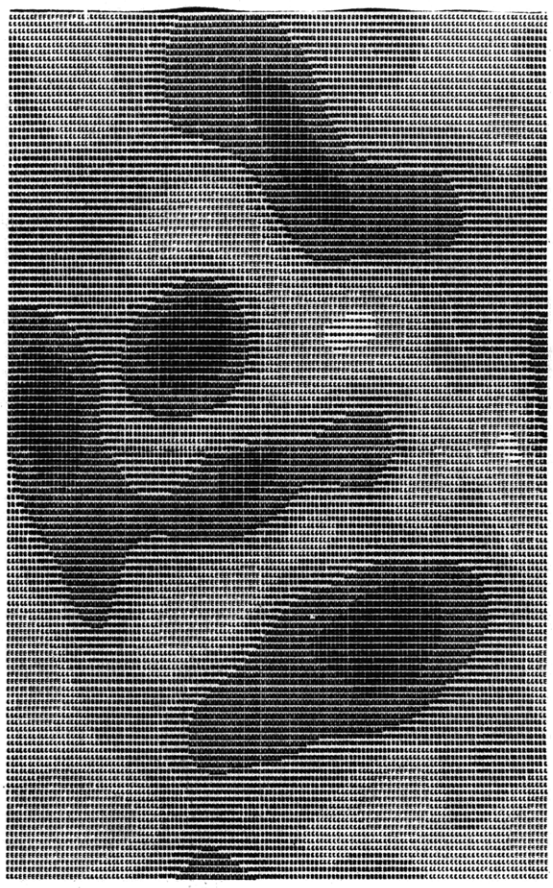

a(x,y)

(filtered and normalized)

Figure 5

2008Z

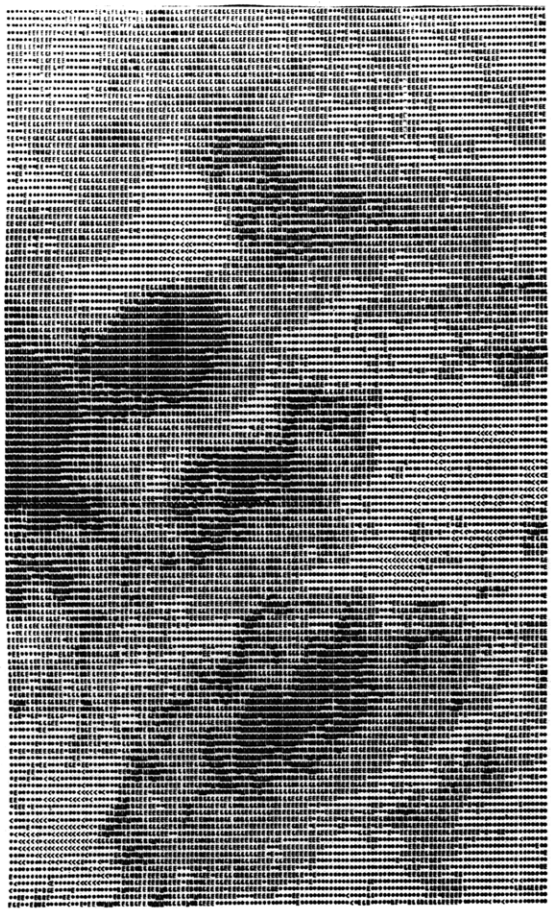

b(x,y)

(normalized)

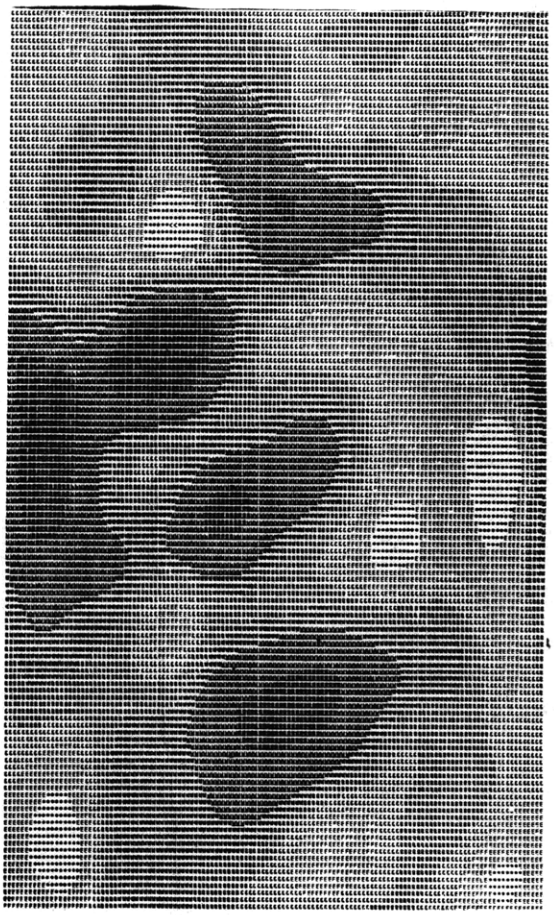

b(x,y)

(filtered and normalized)

Figure 6

2208Z

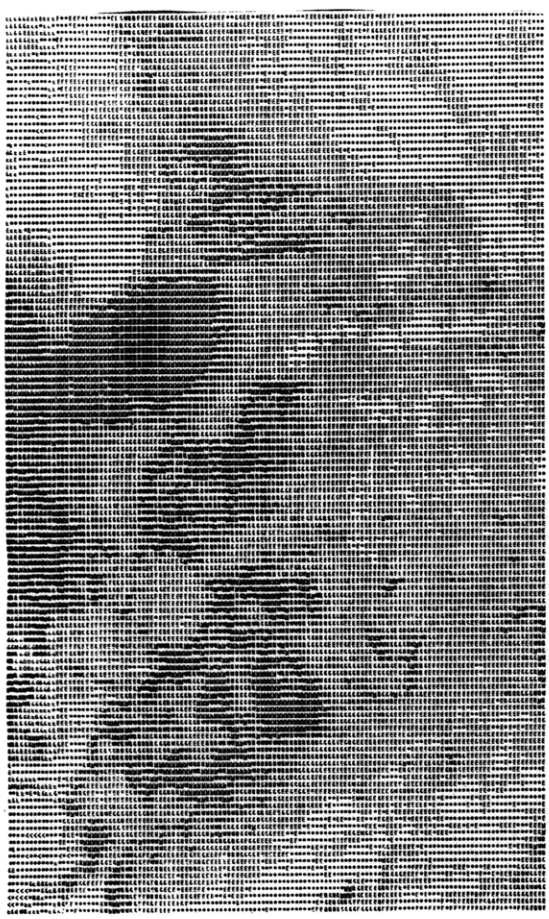

$c_v(x,y)$

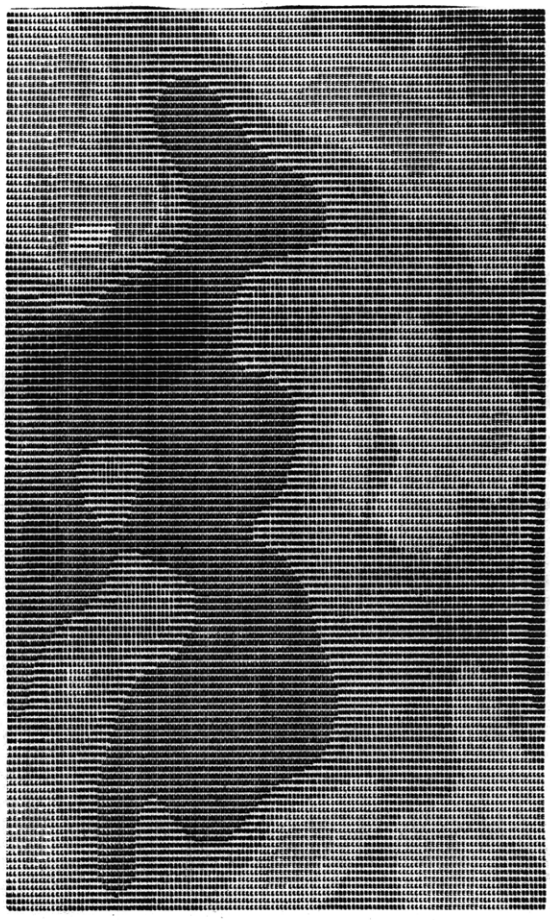

$c_v(x,y)$

(filtered)

Figure 7

FORECASTS FOR 2208Z

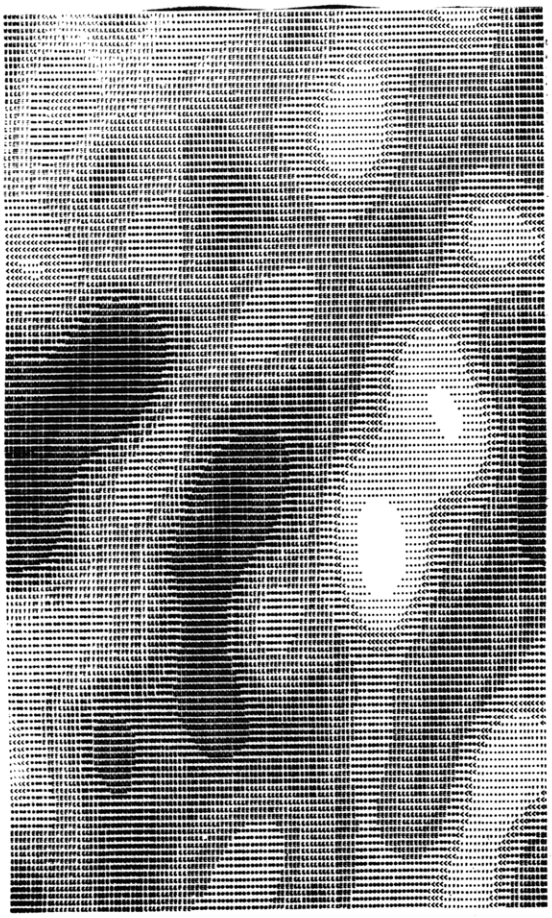

$c_p(x,y)$ (K=1)

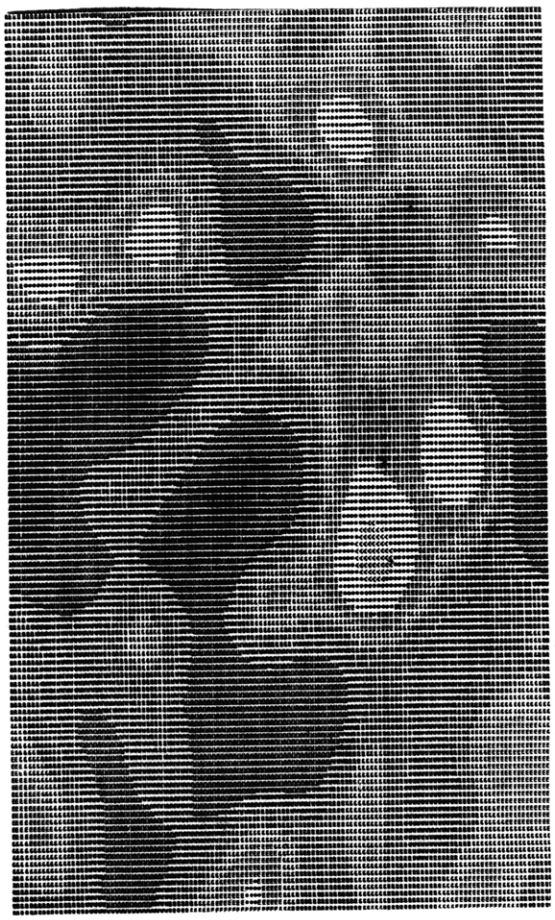

$c_p(x,y)$ (K=0)

Figure 8

SERIES OF ATS-I SATELLITE PHOTOGRAPHS

14 August 1971	2147Z
15 August 1971	1809Z
	1833Z
	1857Z
	1921Z
	1944Z
	2008Z
	2032Z
	2056Z
	2120Z
	2144Z
	2232Z
	2255Z
16 August 1971	2154Z

Table 1

METEOROLOGICAL OBSERVATIONS AT JOHNSTON ISLAND - 15 August 1971

	Surface Wind		Three-hour pressure
GMT	Direction	Speed(Knots)	tendency(tenths of millibars)
00	SE	10	-10
06	ENE	10	+ 8
12	E	10	- 8
18(sun-rise)	ESE	10	+ 7

Table 2

RELATIVE FORECAST ERRORS

Climatology	8,648
Persistence	4,643
Prediction K=1	15,135
Prediction K=0	5,422

Table 3

ACTUAL MOTION OF 3 CLOUD BANDS (BASED ON MOTION IN KNOTS OF CENTERS OF MASS)

	UPPER		MIDDLE		LOWER		AVERAGE(3 bands)	
from	U	V	U	V	U	V	U	V
A to B	-12	-5	-12	-5	-55	-15	-26	-8
B to C	-12	+7	-12	-7	-30	- 2	-18	-1
B to $C_{k=1}$	-30	+5	- 2	0	-25	- 2	-19	+1
B to $C_{k=0}$	-25	-5	- 2	+2	-17	- 5	-15	-3

Where U is positive to the east and

V is positive to the north

ESTIMATED PHASE SPEED OF IMAGE (via method on P. 28)

Westward at approximately 6 knots.

CLIMATOLOGICAL AVERAGE SPEED OF TROPICAL DISTURBANCES (Reed and Recker, 1971)

Westward at 18 knots.

Table 4

BIBLIOGRAPHY

1. Anuta, Paul E., "Spatial Registration of Multispectral and Multitemporal Digital Imagery Using Fast Fourier Transfer Techniques", IEEE Transaction on Geoscience Electronics, Oct. 1970, pp 353-368.

2. Bluestein, Howard B., Unpublished(work at NHRL; Miami, Fla.) Summer 1971.

3. Boucher, Roland J., "Relationships Between the Size of Satellite-Observed Cirrus Shields and the Severity of Thunderstorm Complexes", JAM, Vol. 6, No. 3, June 1967, pp 564-572.

4. Endlich, R.M., Wolf, D.E., Hall, D.J., Brain, A.E., "Use of a Pattern Recognition Technique for Determining Cloud Motions from Sequences of Satellite Photographs", JAM, Vol. 10, No. 1, Feb. 1971, pp 105-117.

5. Frank, Neil L., "The 'Inverted V' Cloud Pattern -- An Easterly Wave?", MWR Vol. 97,No. 2, Feb. 1969, pp 130-140.

6. Gold, Bernard, Rader, Charles M., Digital Processing of Signals, McGraw-Hill, 1969.

7. Huang, T.S., Schreiber, W.F., Tretiak, O.J., "Image Processing", Proceedings of the IEEE, Nov. 1971, pp 1586-1609.

8. Hubert, L.F., Whitney, L.F., Jr., "Wind Estimation from Geostationary-Satellite Pictures", MWR, Vol. 99, No. 9, Sept. 1971, pp 665-672.

9. Leese, John A., Epstein, Edward S., "Application of Two-Dimensional Spectral Analysis to the Quantification of Satellite Cloud Photographs", JAM, Vol. 2, No. 5 , Oct. 1963, pp 629-644.

10. Leese, John A., Novak, Charles S., Taylor, V. Ray, "The Determination of Cloud Pattern Motions from Geosynchronous Satellite Image Data", Pattern Recognition, Pergamon Press 1970, Vol. 2, pp 279-292.

11. Leese, John A., Novak, Charles S., Clark, Bruce B., "An Automated Technique for Obtaining Cloud Motion from Geosynchronous Satellite Data Using Cross Correlation", JAM, Vol. 10, No. 1, Feb. 1971, pp 118-132.

12. Noel, Thomas M., Fleisher, Aaron, "The Linear Predictability of Weather Radar Signals", M.I.T. Dept. of Meteorology, Cambridge, Mass., Research Report No. 34.

13. Reed, Richard J., Recker, Ernest E., "Structure and Properties of Synoptic-Scale Wave Disturbances in the Equatorial Western Pacific", JAS, Vol. 28, No. 7, Oct. 1971, pp 1117-1133.

14. Robbins, Gregory Manson, The Inversion of Linear Shift-Variant Imagery Systems, Ph.D. Thesis, M.I.T. Dept. of Electrical Engineering, Aug. 1970.

15. Sikdar, D.N., Suomi, V.E., "Time Variation of Tropical Energetics as Viewed from a Geostationary Altitude", JAS, Vol. 28, No. 2, March 1971, pp 170-180.

16. Wallace, J.M., "Time-Longitude Sections of Tropical Cloudiness(December 1966 - November 1967)", July 1970, ESSA Tech. Report NESC 56.

ACKNOWLEDGMENTS

Thanks must go to my thesis advisors, Professor Frederick Sanders and Professor Edward Lorenz of the Department of Meteorology, and to Dr. Oleh Tretiak of the Electrical Engineering Department, Massachusetts Institute of Technology, Cambridge, Mass. for their encouragement and guidance.

Special thanks are due to Jim Harrison and Dr. John Leese of the National Environmental Satellite Center for supplying the satellite photographs and tapes; to Joe Chase of the Woods Hole Oceanographic Institute for supplying surface synoptic weather maps for the forecast area; to Bob Crosby for programming assistance; to Isabelle Kole for typing the first draft and drawing the figure; and to Kate Higgins for typing this manuscript.

This work was done in part at the M.I.T. Information Processing Center. The research was supported by NOAA Grant E-2237-71(G).